# Surface Crack Initiation Phenomenon in Very High Cycle Fatigue

## MuhammadKashif Khan[1,*], QingYuan Wang[1]

1 Department of Mechanics and Engineering Science, Sichuan University, Chengdu 610065, China.
* Corresponding author: email@address.aa.b.cc

**Abstract**   Very High Cycle Fatigue behavior of Stainless Steel AISI 310 has been investigated through ultrasonic fatigue testing. In fatigue cycles, a horizontal asymptote of S-N curve was found without any step at $10^6$ cycles. Surface crack initiation was found irrespective of the stress level. However, the fracture surfaces of the material showed different behavior of crack propagation for different stages of fatigue cycles. It was found that up to $10^6$ cycles, cracks initiated from surface defects and carbide precipitates present on the grain boundaries. The mechanism of crack initiation changed at low stress levels and slip bands and deformation twins were found at the surface of the specimen which acted as fatigue crack initiation sites. At lower stress levels, at or below fatigue limit, PSBs were developed but the cracks were not initiated. The lower slope in S-N curve was attributed to the development of PSBs all over the surface of the specimen before crack initiation.

**Keywords**   Very high cycle fatigue, Crack initiation , PSBs, Local plasticity

## 1. Introduction

The fatigue crack initiation and growth in metallic materials is now well-understood. Fatigue cracks initiate at stress concentrating features within a structure. An area of fatigue assessment is still under investigation, however, is how cracks are initiated from surface and subsurface regions at very low stress levels in the very high cycle fatigue (VHCF). It is believed that the fatigue life of numerous aerospace, locomotive, automotive and biomedical structures may go beyond $10^8$ cycles [1]. Hence, better understanding of the long life fatigue behavior is extremely important for efficient design of the components and structures, especially between the $10^7$-$10^{10}$ cycles. Most engineering designs were based on the assumption that materials exhibit a fatigue limit and any cyclic stress below fatigue limit yield infinite life. Recent studies, however, point out the fact that most materials experience failure up to $10^{10}$ cycles or above at low stress levels, and concept of infinite fatigue life is not true [1-4].

The VHCF behaviour of metallic materials is generally divided in two types, based on the crack initiation region [1-4]. In first type, the cracks are initiated from the internal defects of the material and a fish-eye region is obtained at the crack initiation site. In second type, the cracks are initiated from the surface of the material. These surface cracks are attributed to the surface defects, heterogeneities, pores and absence of inclusions and microstructural defects in some other materials. In this type of materials, the S–N curve between $10^6$ to $10^9$ cycles show very little decreasing slope without any transition at $10^7$ cycles and horizontal asymptote is obtained.

The VHCF behavior of some materials shows subsurface crack initiation from the internal defects and inclusions [4]. However, surface crack initiation is also obtained in structural alloys which show no inclusions and microstructural defects [5-7]. Plastic deformations at localized regions initiate the fatigue cracks during cyclic loading. During fatigue loading, the stress concentration due

to the induced microscale plasticity around surface defects and pores [5], planar slip bands [6] and grain boundaries [7], results in crack initiation. The crack initiation site for these materials remains at the surface of the specimens, even for higher fatigue cycles from $10^8$ to $10^9$ cycles. The most common plastic deformation in FCC materials is the development of Persistent Slip Bands (PSBs) which yields intrusions and extrusions on the surface of specimens. In this case, the S–N curve decreases linearly with very little slope without transition at $10^7$ cycles [3].

One important structural material which show surface based crack initiation is high temperature grade stainless steel alloy AISI 310. The alloy is very commonly used in moist conditions owing to its excellent characteristic to resist against corrosion. It is used in heat exchangers, pipes, machinery parts etc. The alloy is subjected to pressure cycles, temperature cycles and many start up and shut down cycles during service life. Hence, it is expected to serve for large number of loading cycles. However, there is no such study for this material, to the best of authors' knowledge, which details the behavior of fatigue crack initiation phenomenon especially up to very high cycle fatigue domain. Hence, it is important to be able to assess the very high cycle fatigue behavior of the material.

The surface crack initiation phenomenon even at lower stress levels has been studied previously and different conclusions have been made. Tokaji et al. [8] and Yang et al. [9] in Mg alloys, Miura et al. [10] and Sakai et al. [11] in steels studied the surface based crack initiation. The surface cracks initiation has been attributed to micro-cracks [12], surface roughness [13] and, intrusions and extrusions [14]. In addition, few efforts have been made to characterize the nature of PSBs in range of materials. Man et al. [15] studied the difference in the topography of slip bands in FCC and BCC materials. Polak et al. [16-17] studied the different stainless steels and attributed the local plasticity due to the intrusions and extrusions and their interaction with nearby heterogeneities, for the fatigue crack initiation. The localized plastic deformation and surface roughness developed in fatigue loading, and their interaction with surface defects have been attributed for the surface based crack initiation. It has been concluded that any or combination of these parameters may initiate cracks from the surface of the specimens. However, the crystallographic orientations of the grains play major role in the surface crack initiation. Owing to the difference in basal slip and twining mechanism for FCC and HCP based crystal structure, difference in the topography of PSBs is obtained. Hence, case by case experimental investigation of the crack initiation region and slip and basal planes for different materials is considered inevitable.

Ultrasonic fatigue testing has been used in this study to investigate the VHCF behaviour of Stainless Steel AISI 310. The S-N curve showed horizontal asymptote without any step at $10^6$ cycles. Surface crack initiation was found irrespective of the stress level. However, the fracture surfaces of the material showed different behavior of the crack propagation for different stages of the fatigue cycles. It was found that up to $10^6$ cycles, the cracks initiated from carbide precipitates present on the grain boundaries. The mechanism of crack initiation changed at low stress levels and PSBs were observed at the surface of the specimen which acted as the fatigue crack initiation sites.

The main aim of this study is to enhance the VHCF life of metallic materials though surface modification techniques like Ultrasonic Nanocrystal Surface Modification (UNSM). A precursor to this goal is better understanding of VHCF behaviour of the material. The surface crack initiation for AISI 310 makes it an ideal material for the application of UNSM. The materials which exhibit subsurface crack initiation, the application of compressive residual stresses may enhance the

subsurface crack initiation owing to the compensatory tension. Hence, it is anticipated that VHCF life of AISI 310 can be enhanced due to UNSM.

## 2. Materials and Experimental Methods

Cold rolled cylindrical rods of 12mm diameter of AISI 310 were used in this study. AISI 310 is a commonly used material in heat exchangers, pipes and machinery parts. The material exhibits excellent high temperature properties with good ductility and weldability. It resists oxidation at elevated temperature and corrosion in moist conditions and dry environments.

Metallographic sample were prepared up to 0.05 micron finish and etched with Aqua Regia Reagent (15 mL HCL + 5 mL $HNO_3$ + 100 mL $H_20$) for 120 sec. The grain size of the material was determined by quantitative metallography and was found to be ~10 um as shown in Fig. 1. The grains were equiaxed and showed a random orientation. Carbide particles were obtained on the grain boundaries of the material. Elastic–plastic properties of the material were obtained by tensile testing according to ASTM standard E8 and are given in Table 1. Vickers microhardness tester was used at 200g load. The average Vickers hardness of the material was found as 370HV.
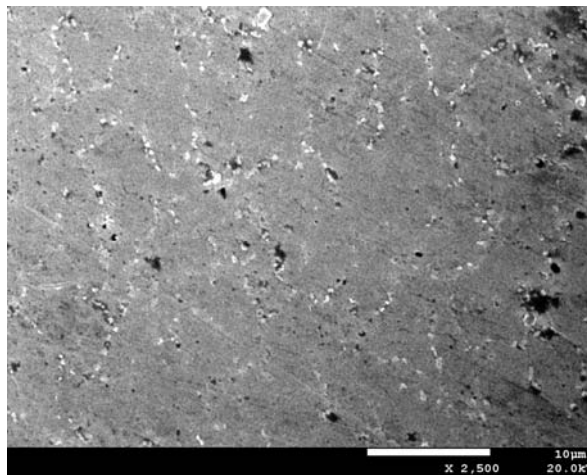


Figure 1. SEM Micrograph of the material. Carbide precipitates are prominent on the grain boundaries

Table 1. Mechanical property data for AISI 310

| Material | E (GPa) | $\sigma_y$ (MPa) | Gauge length (mm) | Hardness (HV) | E / $\sigma_y$ |
|---|---|---|---|---|---|
| AISI 310 | 205 | 850 | 25 | 370 | 240 |

The chemical composition of the material is shown in Table 2. X-ray diffraction (XRD) was used to obtain the details of the diffracting planes and their preferred orientation. Diffraction planes (111), (200) and (220) were obtained for the material. The crystallographic orientations of diffracting planes were measured and it was found that the grains were randomly oriented without any preferred orientation. More details of the XRD and texture results can be found elsewhere [18].

Table 2. Composition of AISI 310 steel

| Material | C% | Cr % | Ni % | Si % | Mn % | Cu % | Mo% | P% | Fe % |
|---|---|---|---|---|---|---|---|---|---|
| AISI 310 | 0.04 | 23.3-23.4 | 18.9- | 1.8 - | 1.21 - | 0.3 | 0.13-0.15 | 0.03 | Bal |

| | | | 18.1 | 1.9 | 1.27 | | | | |
|---|---|---|---|---|---|---|---|---|---|

The VHCF testing samples were designed to resonate longitudinally at 20kHz with the ultrasonic fatigue testing system. The detailed geometrical size of the specimens is shown in Fig. 2. The surface of the specimens was polished to surface roughness 0.2 um. Surface roughness of the material was determined with Atomic force microscope (AFM). Surface roughness Ra for different regions were measured and found up to 80nm.
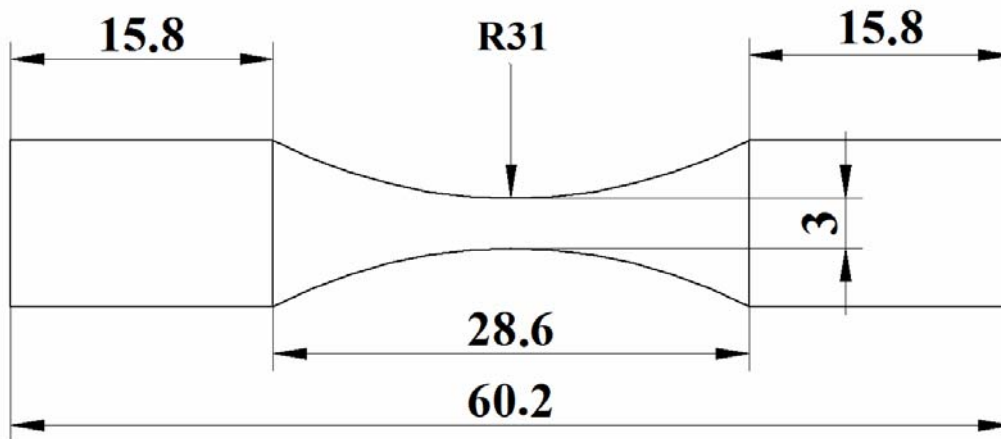


Figure 2. Schematic representation of fatigue specimen

## 3. Results and Discussion
## 3.1- S-N Curve

Fig. 3 shows the S-N curve for the material. The curve showed a higher decreasing slope at higher stress levels up to $10^6$ cycles. This showed that at higher stress levels, the fatigue life was continuously decreasing. A semi-asymptote type curve was obtained and the curve became almost horizontal after $10^6$ cycles. This was in agreement with earlier studies where a horizontal curve was reported for stainless steels [3, 10]. The material showed fatigue limit at around 500MPa and exhibited run out samples. It was found that the fatigue fracture for this material can occur beyond $10^7$ cycles up to $10^9$ cycles, though the difference in the fatigue strength was only around 50MPa.
The little difference in fatigue strength between $10^6$ to $10^9$ cycles and lower slope of S-N curve may be attributed to the relatively lower UTS of the material [3]. It was found that owing to the lower slope, little difference in stress levels changed the failure cycles significantly. This showed that fatigue crack initiation and propagation at relatively lower stress levels required considerable increase in the fatigue cycles to yield a failure. On the other hand, this showed that for a very small increase in stress level, the fatigue cycles would reduce significantly. The difference in stress levels for fatigue life between $10^6$ to $10^8$ cycles was almost 30MPa. For engineering applications, where materials are designed to serve $10^7$ to $10^8$ fatigue cycles, only increase in 30MPa may reduce the fatigue life from $10^6$ to $10^8$ cycles, which is significant.
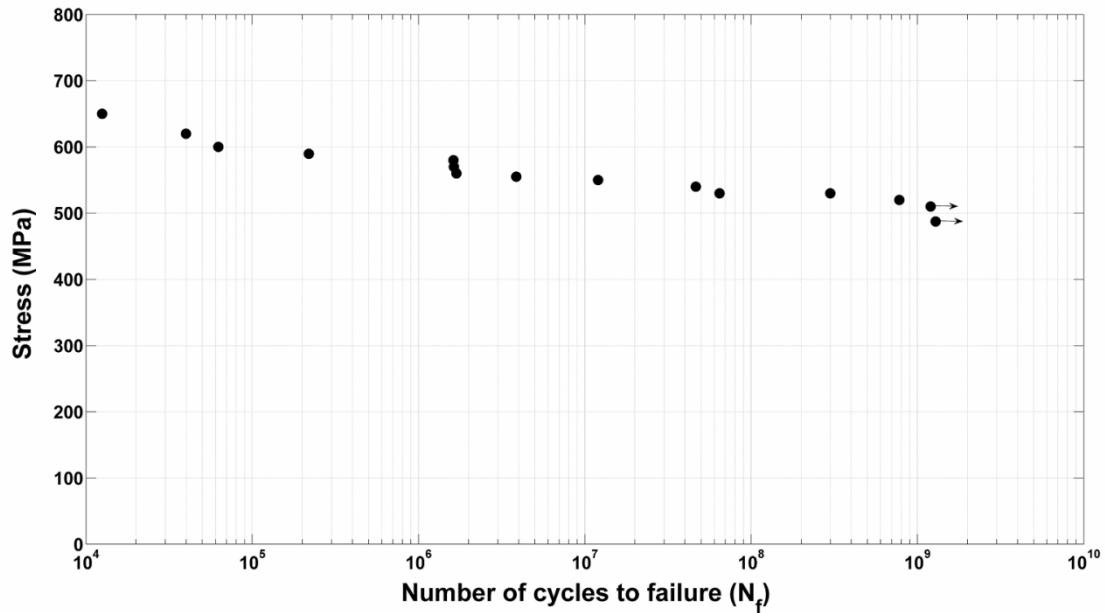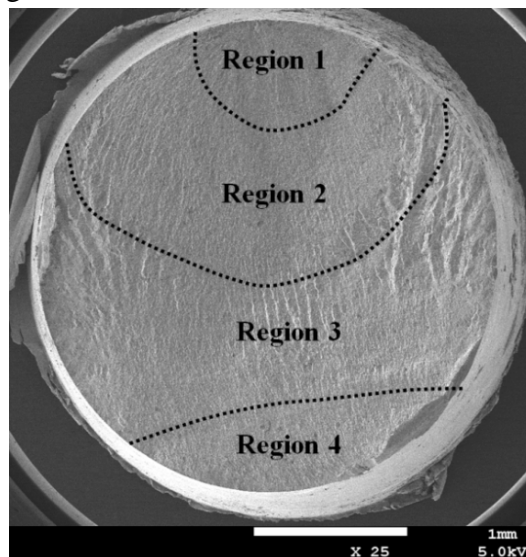
Figure 3. S-N curve for the material

## 3.2 Fractography

Scanning Electron Microscope (SEM) was used to observe the fatigue crack initiation sites and the fracture surfaces. It was observed that for all smooth and notched specimens, the cracks initiated from the surface of specimens, even at VHCF cycles.

Fig. 4 (a) shows the cross-section of the fracture surface of the specimen failed at $7.78 \times 10^8$ cycles when loaded at 520MPa. It can be seen that the appearance of fracture was different at different locations and based on the appearance, four different regions were visible. Radial patterns of striations were observed having 110 to 130um spacing between each other. The initiation site was a localized region on the surface of the specimen. Fig. 4 (b) shows the crack initiation region and crack propagation direction from the surface of specimen. The striations started from the crack initiation site and extended to more than three-quarter of the surface of specimens. The details about the regions are discussed elsewhere [18]. Cleavage fracture was observed with many secondary cracks and higher surface roughness.
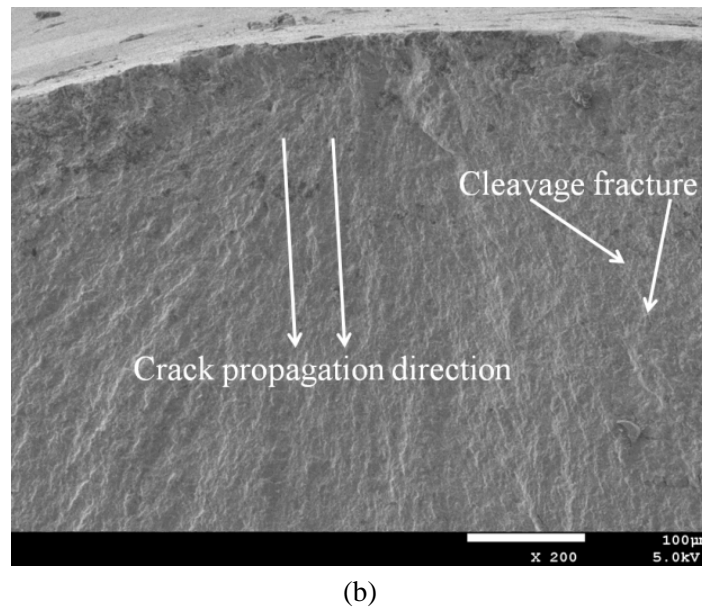


(a)

(b)

Figure 4. Fracture surface (a) sample failed at $7.78 \times 10^8$ cycles (b) Crack initiation from the surface

## 3.3 Fatigue Crack Initiation

It is well known that due to fatigue loading the cracks initiate from the localized plastic deformation [9]. For FCC materials, the local plasticity develops in the form of PSBs and twining and induces surface crack initiation. So far different conclusions have been made in the past for the surface based crack initiation phenomenon [8-11]. The changes in the microstructure, slip system, twin bands and surface defects have been attributed to the crack initiation in different materials. In this study, it was revealed that the mechanism of fatigue crack initiation at different fatigue loading cycles was different depending upon the stress levels. However, the initiation region was always found on the surface of the specimen.

The surfaces of the fractured specimens, parallel to the loading direction, were investigated through the SEM and AFM. The specimens failed at higher stress levels up to $10^6$ cycles showed smooth surface without having any slip markings. No damage or sign of local plastic deformation was observed. The crack initiation site was very localized region at the surface of the material with no nearby damage. This showed that the carbide particles at the grain boundaries, as found in earlier studies, acted as stress concentration regions for crack initiation [15].

However, the specimens failed beyond $10^6$ cycles showed high density PSBs and deformations on the surface. Fig. 5 shows SEM image of the surface of specimen failed at $3 \times 10^8$ cycles. It can be seen that high density slip bands were all over the periphery of the specimen. The near fracture surface showed more number of PSBs. The majority of the dislocations were parallel to the loading directions which were wider and broader as compared to the others. However, some dislocations were observed transverse to the loading directions as well.
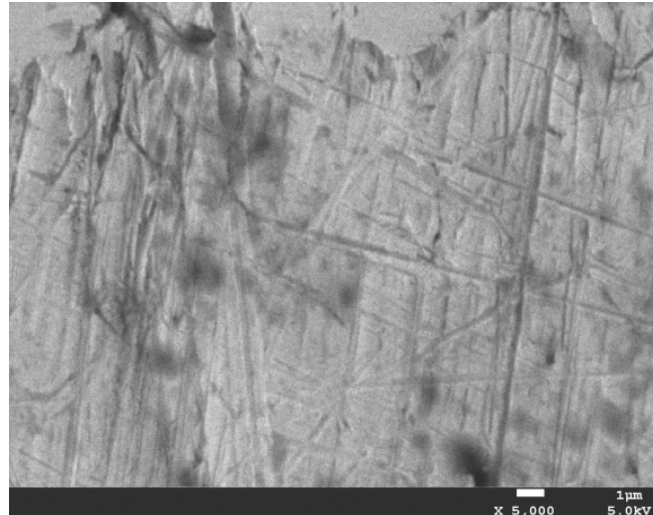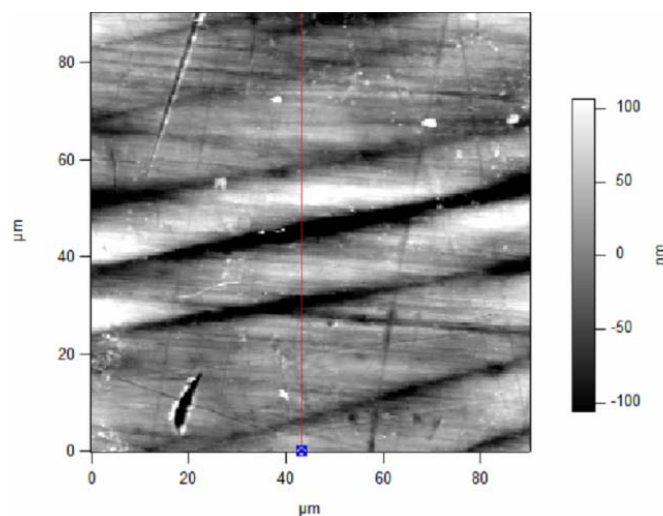
Figure 5. PSBs and dislocations on the surface of specimen failed at $3 \times 10^8$ cycles (520MPa)

The surface parallel to the loading direction of other specimens were also investigate and it was found that the PSBs started to emerge out after $10^6$ cycles on the surface of specimens. The density of PSBs continuously increased with further fatigue cycles [11]. With increase in the fatigue cycles, the topography of the PSBs enhanced. Longer, deeper and broader slip bands were obtained for higher fatigue cycles which increased the surface roughness of the specimen. The surface roughness of the specimens was measured as 178nm and 247nm for the specimen failed at $6.45 \times 10^7$ and $7.78 \times 10^8$ cycles respectively. This showed that the additional fatigue cycles after $10^6$ cycles were utilized in the creation of PSBs at the surface of the specimen.

The topography of PSBs was investigated in detail through AFM. PSBs were present in the form of shallow intrusions and extrusions. Fig. 6 (a) shows 90um x 90um size AFM scanned image of a near fracture region in specimen failed at $3 \times 10^8$ cycles. Fig. 6 (b) shows the 3D image of the area. The topography of intrusions and extrusions was like shallow scratches and waves, respectively [15-17]. Fig. 6 (c) shows the height profile data from the top corner of the area through the slip bands to the other corner of the area (shown by the red line in Fig. 6 (a)) showed many different crust and troughs. Several combinations of intrusions and extrusion, parallel to each other, were observed [16-17]. The distance between intrusions and extrusions was very small and maximum depth of the slip bands reached to around 250nm in some regions.
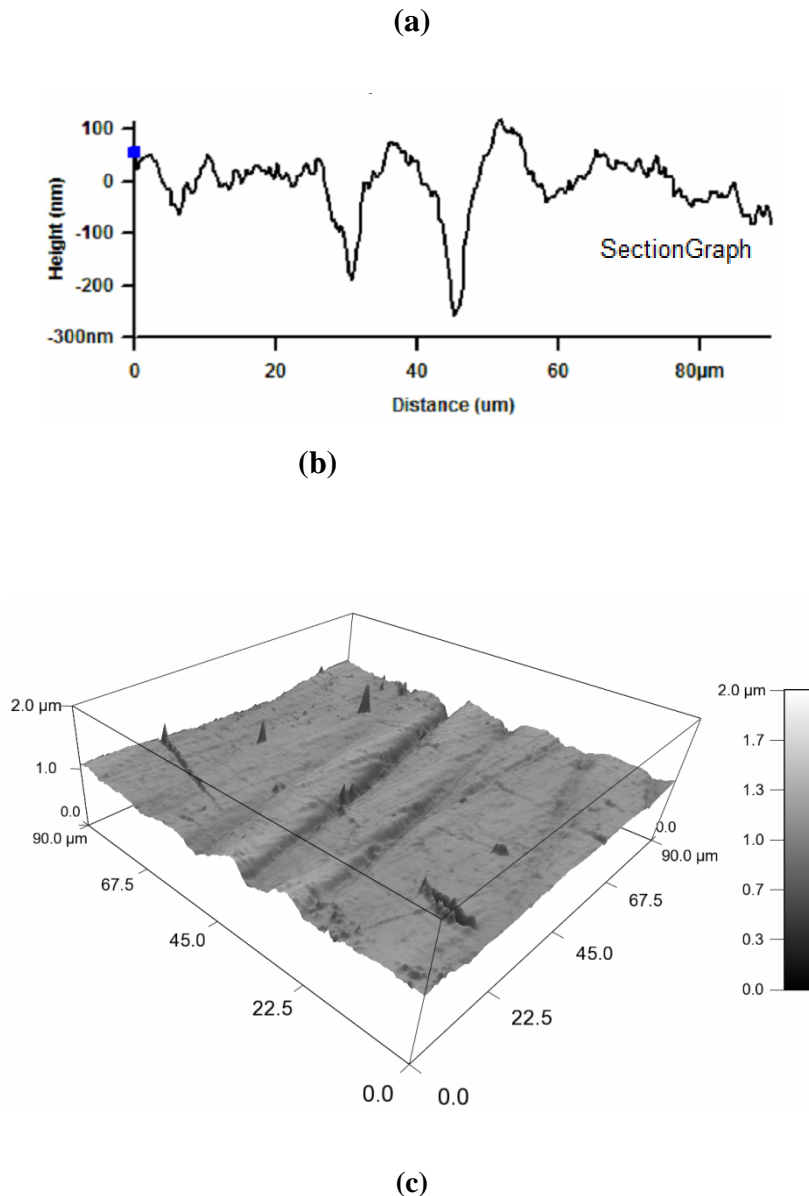
**(a)**

**(b)**



**(c)**

Figure 6 (a) AFM scanned image of an area near to crack initiation for the specimen failed at $3 \times 10^8$ cycles (b) height profile through the area (from one corner to the other corner) showing significant PSBs and dislocations (c) 3D surface topography of the region

The process of utilization of additional fatigue cycles for the creation and enhancement of PSBs explains the large difference in fatigue failure cycles for very small decrease in the stress levels. At lower stress levels, development of PSBs and their subsequent enhancement required significantly higher fatigue cycles. However, for higher slope S-N curves, only small subsurface region is affected from the localized plasticity, hence relatively smaller difference in the fatigue cycles are usually required for any small decrease in the stress value.

FCC materials are known to show PSBs under loading [19]. The main slip system for the material was FCC structure (111) [18]. When the material was fatigue loaded, the crystal plane (111) with higher Schmid factor suffered from the higher degree of plastic deformation. The strains get localized due to the dislocation accumulation at grain boundaries of the material [11]. The interaction of precipitates at the grain boundaries of the material having higher Schmid factor with the dislocations started to occur [9, 15]. The partial surrounding of the grains at the leading surface of specimen [9] and this interaction in combination, not only generated the PSBs and local yielding

at the surface of the material, but also increased the surface roughness.

The local stress concentration created due to the sharp edges of PSBs act as the crack initiation and propagation [8, 14-15]. The slip markings developed due to the dislocation accumulation, transformed into the PSBs in the form of extrusions and intrusions. The deepest intrusion PSBs act as the potential fatigue crack initiation and propagation region [11, 15-17].

The fatigue failure with and without PSBs for specimens failed above and below $10^6$ cycles showed that the fatigue crack initiation was highly dependent on the applied stress. At higher stresses, PSBs were not observed, yet the crack initiation took place from the surface of the specimen. The carbide precipitates were found as the crack initiation sites. However, when the stress levels were reduced, the PSBs played pivotal role in limiting the fatigue life of the material from $10^6$ cycles and above. At further lower stress levels, at or below the fatigue limit, the PSBs were developed but found as non-damaging and the crack initiation was not observed. These PSBs were formed due to the large number of fatigue cycles and the stress concentration due to the lower stress was not sufficient to initiate the crack.

## 4. Conclusions

Fatigue behavior of AISI 310 was investigated up to very high cycles. S-N curve with very small decreasing slope was obtained without any step. It was found that the fatigue fracture can occur beyond $10^7$ cycles in this material.

It was observed that all cracks were initiated from the surface of the specimen irrespective of the stress levels and the cycles before fatigue failure. No fish-eye or subsurface crack initiation was observed.

It was found that at higher stress levels, the specimen exhibited lower fatigue life and cracks initiated from carbide precipitates on the surface of specimen.

However, above $10^6$ cycles at lower stress levels, PSBs were found at the surface of the specimen and acted as the fatigue crack initiation site. Arrays of intrusions and extrusions around the whole periphery of the specimen were observed. The sharp edges of PSBs served as the fatigue crack initiation and propagation.

The lower slope in S-N curve showed that little decrease in stress level increased the failure cycles significantly. The higher fatigue cycles were used in development of PSBs all over the surface of the specimen as compared to the materials exhibit fish-eye failure, which required localized plasticity in subsurface region for initiation of crack.

## 6. References

[1] C. Bathias and P. C. Paris. Gigacycle fatigue in mechanical practice. Taylor & Francis, 2004.
[2] I. Marines, X. Bin, C. Bathias. An understanding of very high cycle fatigue of metals. Int. J. Fat., 25 (2003), 1101–1107.
[3] C. Bathias, L. Drouillac, P. L. Francois. How and why the fatigue S–N curve does not approach a horizontal asymptote. Int. J. Fat., 23 ( 2001), S143–S151.
[4] H. Mughrabi. Specific Features and mechanisms of fatigue in the ultrahigh-cycle regime. Int. J. Fat., 28, 2006, 1501-1508.
[5] C. Stocker, M. Zimmermann, H. Christ. J. Effect of precipitation condition, prestrain and temperature on the fatigue behaviour of wrought nickel-based superalloys in the VHCF range. Acta Mater., 59 (2011), 5288-5304.
[6] S. T Stanzl, H. Mughrabi, B. Schoenbauer. Int. J. Fat., 29 (2007), 2050－2059.

[7] C. R. Sohar, A. Kotas, C. Gierl, B. Weiss. Gigacycle fatigue behavior of a high chromium alloyed cold work tool steel. Int. J. Fa.t, 30 (2008), 1137–1149.

[8] K. Tokaji, M. Kamakura, Y. Ishiizumi Y, N. Hasegawa. Fatigue behaviour and fracture mechanism of a rolled AZ31 magnesium alloy. Int. J. Fat., 26 (2004), 1217-1224.

[9] F. Yang , S. M. Yin, S. X. Li. Crack initiation mechanism of extruded AZ31 magnesium alloy in the very high cycle fatigue regime. Mat Sci. Eng A. 491 (2008), 131–136.

[10] N. Miura, Y. Takahashi. High-cycle fatigue behaviour of type 316 stainless steel at 288 C including mean stress effect. Int. J. Fat., 28 (2006), 1618-1625.

[11] T. Sakai, Y. Sato, N. Oguma. Fat. Fract. Engng. Mat. Struct., 25 (2001), pp 765-773.

[12] Chai G. Fatigue behaviour of duplex stainless steels in the very high cycle regime. Int. J. Fat., 28 (2006), 1611–1617.

[13] I. Marines, G. Dominguez, G. Baudry. Ultrasonic fatigue tests on bearing steel AISI-SAE 52100 at frequency of 20 and 30 kHz. Int. J. Fat., 25 (2003), 1037–1046.

[14] D. K. Xu, L. Liu,Y. B Xua. The crack initiation mechanism of the forged Mg－Zn－Y－Zr alloy in the super-long fatigue life regime. Scripta Mater., 56 (2007), 985-994.

[15] J. Man, M. Petrenec, K. Obrtlik and J. Polak. Acta Mater., 52 (2004), 5551－5561.

[16] J. Polak, T. Kruml, K. Obrtlik and J. Man. Proc. Engng., 2 (2010), 883–892.

[17] J. Polak, J. Man, K and Obrtlik K. Int. J. Fat. 25 (2003), 1027–1036.

[18] Khan M. K.　Wang Q. Y. To be published.

[19] H. Mughrabi, K. Herz, X. Stark. Cyclic deformation and fatigue behaviour of alpha-iron mono- and polycrystals. Int. J. Fract. 17 (1981), 193-220.